Gärtner, Eric ; Jung, Hyo Yun ; Peter, Nicolas J. ; Dehm, Gerhard ; Jägle, Eric A. ; Uhlenwinkel, Volker ; Mädler, Lutz

# Reducing cohesion of metal powders for additive manufacturing by nanoparticle dry-coating

# Reducing cohesion of metal powders for additive manufacturing by nanoparticle dry-coating

Eric Gärtner [a,b], Hyo Yun Jung [c,d], Nicolas J. Peter [c], Gerhard Dehm [c], Eric A. Jägle [c,e], Volker Uhlenwinkel [a,b], Lutz Mädler [a,b,*]

[a] Leibniz Institute for Materials Engineering IWT, Badgasteiner Strasse 3, 28359 Bremen, Germany
[b] University of Bremen, Faculty of Production Engineering, Badgasteiner Strasse 1, 28359 Bremen, Germany
[c] Max-Planck-Institut für Eisenforschung GmbH, Max-Planck-Strasse 1, 40237 Düsseldorf, Germany
[d] Korea Institute of Industrial Technology, Jongga-ro 55, 44413 Ulsan, Republic of Korea
[e] Universität der Bundeswehr München, Institute of Materials Science, Werner-Heisenberg-Weg 39, 85577 Neubiberg, Germany

ARTICLE INFO

*Keywords:*
Powder flowability
Additive manufacturing
Dry-coating
Nanoparticles

ABSTRACT

Additive manufacturing processes, such as laser powder bed fusion, require steady powder processing but often exhibit poor flowability and low powder bed densities. Reducing the attractive Van-der-Waals force through nanoparticle coating can enhance initially poor flowability. We investigated the effect of dry-coating nanosized $SiO_2$ on gas-atomized CoCrFeNi powders containing different amounts of particles $< 20$ μm with respect to nanoparticle concentration and mixing time. The dynamic angle of repose of a 0–90 μm powder reduced 50% and bulk powder density increased 30% with nanoparticle concentrations up to 0.153 wt.-%. The granular Bond-number was correlated with the powder flowability and porosity. The effect of mixing time was investigated with mixing two fractions 20–90 μm and 0–90 μm at a constant nominal nanoparticle surface area coverage of 128% for 2 to 1440 min. Short mixing times improved the flowability, while extensive mixing resulted in nanoparticle reagglomeration and deteriorated flow.



## 1. Introduction

Laser powder bed fusion (LPBF) is a powder-based additive manufacturing (AM) technology that has gained increasing industrial and scientific attention due to its unique advantages, such as high geometrical component freedom and additional product functionality [1–3]. LPBF is nowadays frequently used for prototyping and the production of single components.

Metallic parts are synthesized with layer wise distribution of metal powders and subsequent laser fusion. For a high product quality, unimpeded powder flow is an essential powder property, which decisively ensures stable and reproducible processing [4]. According to Geldart [5] powders can be classified into four groups based on their gas-solid fluidization: group A-aeratable, B-bubble-ready, C-cohesive and D-spoutable. The powder handling behavior is dependent on the density ratio of particles and ambient gas-phase and average particle size. Group C and A are particularly relevant for AM, as common AM powders with a particles size of 40–100 μm and a good flowability can often be assigned to group A [6]. However, particle interaction forces increase with decreasing particle size. This leads to an increasingly cohesive behavior. Powder processing of group C particles is therefore considerably more critical and becomes a challenging task under LPBF conditions [7]. Powder metallurgy companies usually provide feed materials for AM produced with gas atomization processes ranging from 1 to 200 μm. For LPBF, these powders are further fractionated (e.g. 20–63 μm for lightweight materials and 10–45 μm for heavier metals) to ensure the powder processability of Geldart group A for LPBF processing.

It is known from other industrial powder applications, such as pharmaceutical and food processing [8–10], that the flowability of particulate materials is a complex interaction of powder characteristics such as particle size distribution (PSD), particle morphology, surface chemistry and texture, chemical composition and moisture [11,12]. The resulting powder processing properties such as the flowability depend on the mechanical load applied by the feeding equipment [13]. Particle interactions caused from interparticle forces such as the Van-der-Waals force, local chemical bonds, electrostatic charges and liquid bridging of adsorbed secondary substances such as air moisture have a significant influence on powder cohesion and thereby particulate flow [14]. In the absence of capillary or electrostatic forces, a good estimation of the flow behavior or cohesion can be derived from the ratio of the short-range Van-der-Waals attraction force to the inertial force of the powder, introduced by Castellanos [15], also known as the granular Bond-number $Bo_{Granu}$.

* Corresponding author.
*E-mail address:* lmaedler@iwt.uni-bremen.de (L. Mädler).

**Nomenclature**

| | |
|---|---|
| AM | Additive manufacturing |
| LPBF | Laser powder bed fusion |
| PSD | Particle size distribution |
| $AJ$ | Hamaker-constant |
| a | Fitting parameter |
| b | Fitting parameter |
| $Bo_{Granu}$ | granular Bond number |
| $D_{1,2}$ m | Sauter-mean diameter |
| $D_G$ m | Guest-particle diameter |
| $D_H$ m | Host-particle diameter |
| $D_{G,aggl}$ m | Agglomerated guest-particle diameter |
| $H_0$ m | Contact distance |
| $F_G$ N | Gravitational Force |
| $F_{VdW}$ N | Van-der-Waals Force |
| $g$ m/s$^2$ | Gravitation constant |
| $m_H$ kg | Host powder mass |
| $M_{k,t}$ | Moment of the particle size distribution |
| m | Fitting parameter |
| n | Fitting parameter |
| $Q_3$ | Cumulative size distribution |
| $SAC_{nom}$ | nominal surface area coverage |
| $SAC_{real}$ | real surface area coverage |
| $S_G$ m$^2$ | Projection area of guest-particles |
| $S_H$ m$^2$ | Host surface area |
| $S_{H,m}$ m$^2$/kg | Mass-specific host surface area |
| $t_{mix}$ min | Mixing time |
| $v$ vol.-% | Volume concentration |
| V m$^3$ | Volume |
| $w$ wt.-% | Weight concentration |
| $x$-$y$-$z$ m | Scan directions |
| $z_0$ m | Minimal contact distance |
| $\alpha$ ° | Dynamic angle of repose |
| $\rho_B$ kg/m$^3$ | Bulk powder density |
| $\rho_G$ kg/m$^3$ | Guest material density |
| $\rho_H$ kg/m$^3$ | Host material density |
| $\varepsilon$ | Powder porosity |
| $\sigma$ | Geometric standard deviation |

$$Bo_{Granu} = \frac{F_{VdW}}{F_G} = \frac{F_{VdW}}{\frac{\pi}{6} g \rho_H D_H^3} \tag{1}$$

Powders with a higher attractive Van-der-Waals force $F_{VdW}$ than gravity force $F_G$, calculated from the gravity constant $g$, the mean particle size $D_H$ and particle density $\rho_H$, are considered cohesive ($Bo_{Granu} > 1$). If the attraction between particles is lower compared to their specific gravity force ($Bo_{Granu} < 1$), a powder has a rather non-cohesive behavior, typically seen for coarse particles of Geldart group A and B [9]. Based on this consideration, it is evident that particle size plays a prominent role in the flow of a powder. However, if the particle size and shape are invariable within the process, one can only modify the particle surface chemistry or surface morphology to alter the flow behavior [11]. Surface modification processes such as nanosized coating of the micron sized particles is possible with dry-coating [16] or suspension-processing [17]. These processes change the particle's surface roughness and show a significant effect on the particle interaction [18]. Such adhesively bonded nanoparticles then act as artificial roughness separating interacting particles and lowering the particle distance-dependent Van-der-Waals force. Thereby they are considered as flow regulators. Therefore, the cohesiveness of a powder can be altered with dry-coating of a material, thereby reducing $Bo_{Granu}$ towards the non-cohesive regime. Dry-coating aims at overcoming the operational difficulties of cohesive powder handling.

Decisive for the effectiveness of the coating are the technology used, the size of the adsorbed nanoparticles and their surface energy. In a detailed article Sharma and Setia [14] summarized many different types of dry-coating processes and their process-specific effects on the coating quality. Based on the magnitude of energy input, a basic distinction can be made between low, medium and high shear mixing [19]. As an example, Sunkara and Capece [20] showed how high shear mixing with a vibratory mixer compared to a low shear Turbula mixer leads to a more uniform distribution of hydrophobic $SiO_2$ on various host materials. More efficient deagglomeration, dispersion and uniform distribution on the host material led to an improved flowability of the binary mixtures. Both the used mixing technology and the chemical nature of the guest- and host-particles have significant effects on flowability. Huang, et al. [21] and Capece, et al. [9] investigated the interplay of surface energies between guest- and host-particles. The silanization of host-particles led to different degrees of hydrophobic interactions and therefore reduced the $Bo_{Granu}$. Furthermore, hydrophobic host-particles showed an effective reduction of the acting attraction force compared to hydrophilic guest-particles. Yang, et al. [22] also demonstrated a clear improvement in the flowability of corn starch using hydrophobized compared to hydrophobic nanosilica. This was attributed to the reduction of liquid bridges. Zhou and Zhu [6] showed that optimal fluidization and flowability of Geldart Group C powders can be obtained by nanoparticle modification. Crucial criteria are the size and concentration of the deposited guest-particles. Thus, by comparing several studies within the working group, an optimal fluidization was achieved with a surface coverage of 10–20% and a mass concentration of 0.5–1 wt% nanoparticles [23–25].

Chen, et al. [26] and Jallo, et al. [27] calculated $Bo_{Granu}$ of silane surface treated and nanosilica dry-coated alumina particles with direct atomic force microscopy (AFM) interparticle force measurements. Their data correlated with the static angle of repose in a logarithmic manner and was described as a useful index for bulk-level metrics, unfortunately without reporting the correlation values. Capece, et al. [18,28] introduced the power law relationship of Eq.(2) (a and b are fitting parameters) between the flow function coefficient and calculated $Bo_{Granu}$ of microcrystalline cellulose powders dry-coated with hydrophobic $SiO_2$.

$$ffc = a(Bo_{Granu})^{-b} \tag{2}$$

Apart from powder flowability, other powder processing properties are governed by particular interactions. The powder bed porosity $\varepsilon$ is often related to the packing behavior of powders. When a powder is dry-coated with nanoparticles, $\varepsilon$ is calculated from the ratio of the bulk powder density $\rho_B$ and host-particle density $\rho_H$ in Eq. (3).

$$\varepsilon = 1 - \frac{\rho_B}{\rho_H} \tag{3}$$

Yu, et al. [29] generalized the macroscopic packing behavior of smooth glass spheres with microscopic interparticle forces with Eq. (4), were $\varepsilon_0$ is the minimum porosity of a loose or dense powder packing and $m$ and $n$ are fitting parameters. Capece, et al. [9] extended this equation to dry-coated pharmaceutical host-particles with oxidic nanoparticles and found a good agreement between $Bo_{Granu}$ and $\varepsilon$.

$$\varepsilon = \varepsilon_0 + (1 - \varepsilon_0)\, exp\left(-m Bo_{Granu}^{-n}\right) \tag{4}$$

It is useful to generalize both powder flowability and powder packing, as the key process metrics of feedstock materials. Our study uses a similar approach, enabling the quantification of the flowability and lose powder packing through the granular Bond-number.

To this date the concept of nanoparticles acting as flow regulators for poorly flowing metal powders has rarely been reported in the realm of AM technology. Blümel, et al. [30] dry-coated a poly-ethylene powder (45–100 μm) with 0.5 wt.-% of hydrophobic and hydrophilic silica for 10 min. It was shown that the flowability and bulk powder density significantly increase with the addition of nanoparticle. The hydrophobic silica showed a higher effectiveness compared to hydrophilic ones. In a patent Peng, et al. [31] describes the flow improving effect of dry-coating Ni-based metal powders with nanosized $SiO_2$ and carbon black. Using 0.008 wt% hydrophobic silica and a mixing time of 10 min, a fraction 10–45 μm could be well distributed in powder layers. Melnichuk, et al. [32] report a decreasing dynamic angle of repose when using $LaNi_5$ (13–60 μm) dry-coated with hydrophobic nanosized $SiO_2$ between 0.1 and 2 wt.-%. At 0.1 wt.-% the greatest flowability enhancement was found. Further addition of $SiO_2$ showed an increasing dynamic angle of repose. Karg, et al. [33] dry-coated for 1 h different pure aluminum powder fractions below 63 μm with 0.3 wt.-% surface treated hydrophobic nanosized $SiO_2$ for LPBF processing of Al—Cu powder mixtures. The static angle of repose as a measure of flowability was shown to drastically decrease with the additional nanoparticles. The same amount of $SiO_2$ was used for different cohesive powder fractions. In a second study Karg, et al. [16] evaluated the influence of particle size and -morphology of an untreated and dry-coated Al—Si powder on the powder spreadability and LPBF component density. The powders were mixed with 0.5 wt% hydrophilic $SiO_2$ for 15, 30 and 60 min. Depending on the mixing time, after an initial increase in flowability, a deterioration was observed after 30 min mixing of the 20–50 μm fraction. None of the aforementioned publications relate their findings to a minimum nanoparticle concentration depending on the powder size fraction to sufficiently improve the flowability of metallic powders for AM technologies. This work will provide fundamental knowledge of how low nanoparticle concentrations improve the flowability of metallic powders. Moreover, we will show that dry-coating conditioning enables the use of fine particle fractions <20 μm while maintaining sufficient flowability for AM applications.

## 2. Theoretical background

### 2.1. Attraction force models

Powder cohesion is governed by numerous interparticle forces between constituting particles of a powder. A multitude of different mathematical approaches are available for calculating the interaction of particles [34]. The computation of dominant attraction forces aims at understanding and predicting powder handling properties, since fine powders tend to poor processing behaviors. In nanoparticle dry-coating the contact models attempt to predict the interparticle forces between micrometer sized particles acting as a host-particle for adhering nanosized guest-particles. In the absence of capillary and electrostatic force, particle attraction is caused predominantly by the attractive short-range Vander-Waals force $F_{VdW}$ between interacting particles. When two equally sized perfectly smooth host-particles separated by the so-called minimum contact distance $z_0$, the dominant interaction force between the hosts $F_{VdW,H\text{-}H}$ from Eq. (5) is directly proportional to the particle size $D_H$ and the material's Hamaker constant $A_H$ [35].

$$F_{VdW,H-H} = \frac{A_H D_H}{24 {z_0}^2} \tag{5}$$

However, if a particle has a rough surface with radii of curvature, Eq. (5) overestimates the attraction force. Chen, et al. [36] modified the well-known Rumpf [37] model in Eq. (6) and showed that a hemispherical single asperity of guest-particle size $D_G$ between contacting host-particles $D_H$, mimicking a rough particle surface, increases the distance between particles and is thereby able to reduce the net attraction force $F_{VdW,H\text{-}G}$.

$$F_{VdW,H-G} = \frac{A_{H-G}}{12 z_0 2}\left[\frac{3 D_G D_H}{D_G + D_H} + \frac{D_H}{2(H_0/z_0)2}\right] \tag{6}$$

The first term of Eq.(6) accounts for the contact between guest- and host-particle, whereas the second defines the interaction between host-particles at a separation distance $H_0 = z_0 + D_G/2$. When two chemically different materials interact, the Hamaker constant $A_{H\text{-}G}$ is found using Eq. (7) [38].

$$A_{H-G} = \sqrt{A_H A_G} \tag{7}$$

On the basis of the modified Rumpf [37] model, Chen, et al. [36] presented a more realistic approach for calculating the host-particle separation distance $H_0$ in Eq. (8) as a function of the surface area coverage ($SAC$) and therefore locating multiple guest-particles on a globular host-particle surface rather than between opposing surfaces.

$$H_0 = \sqrt{(D_H + D_G)^2 - \left(\frac{1.21}{SAC}\right) {D_G}^2} - D_H \tag{8}$$

The arrangement for a mechanically stable interparticular support of guest-particles between host-particles is described by Zimmermann, et al. [39]. Three guest-particles are individually distributed at the vertices of an equilateral triangle on the host-particle surface. The nominal $SAC_{nom}$ is calculated from the projection area of the guest-particles $S_G$, the number of nanoparticles $N_G$ and the absolute surface of the host-particles $S_H$. The nominal $SAC$ is an accessible parameter that can be helpful in comparing dry-coating processes for different size combinations of guest- and host-particles.

$$SAC_{nom} = \frac{S_G \cdot N_G}{S_H} \tag{9}$$

$$S_G = \frac{\sqrt{3}}{2} {D_G}^2 \tag{10}$$

The projection area $S_G$ of a guest-particle in a hexagonal ordering on the host surface is derived from the average size $D_G$ given for example by adsorption measurements [40].

The absolute host-particle surface is determined from the mass-specific surface area $S_{H,m}$and the powder mass $m_H$, given with the density $\rho_H$ and the Sauter mean diameter $D_{1,2}$ of the host powder.

$$S_H = S_{H,m} \cdot m_H = \frac{6}{\rho_H D_{1,2}} m_H \tag{11}$$

The Sauter mean diameter is a metric accounting for the surface $S$ to volume ratio $V$ of a powder and is calculated from the division of the 3rd and 2nd moment $M_{k,t}$ or reciprocal moment with $k = 1$ and $t = 3$ of the particle size distribution in Eq. (12).

$$D_{1,2} = \frac{6\overline{V}}{\overline{S}} = \frac{M_{3,0}}{M_{2,0}} = \frac{1}{M_{-1,3}} = M_{1,2} \tag{12}$$

Under the assumption that the guest-host-contact of the first term is primarily determined by the guest-particle, Eq. (8) is substituted in Eq. (6) and the attraction force $F_{VdW,H\text{-}G}$ of two uniformly coated host-particles is calculated from the so-called *three-point-contact model* of Eq. (13) [36].

$$F_{VdW,H-G} = \frac{A_{H-G} D_G}{4 z_0 2} + \frac{A_{H-G}}{24 D_H \left[\sqrt{\left(1 + \frac{D}{D_H}\right)^2 - \left(\frac{1.21}{SAC}\right)\left(\frac{D_G}{D_H}\right)^2} - 1\right]^2} \tag{13}$$

At low surface area coverage, the nanoparticle concentration is too low to effectively increase the distance between host-particles. At an increasing number of guest-particles on the host surface, the spacing of the guest-particles in the equilateral triangle reduces and the host-particles depart from each other. The critical guest-particle concentration, determining the onset of the host-particle separation from increasing *SAC* is given in Eq. (14) [41].

$$SAC_{H-G} = \frac{1.21}{1 + 2\left(\frac{D}{D_G}\right)} \tag{14}$$

If the host-particles are coated with an increasing concentration of guest-particles in a hexagonal arrangement, the nanoparticles can precisely submerge into the coating vacancies of the neighboring particle (critical $SAC_{G\text{-}G}$ of 45.3%) [39]. The interaction of the particle system is exclusively determined by guest-guest-contacts. At such high concentrations, $F_{VdW,G\text{-}G}$ is similarly to Eq. (5) calculated with the guest-particle size.

$$F_{VdW,G-G} = \frac{A_G D_G}{24 z_0^2} \tag{15}$$

### 2.2. Guest-particle size effect

To emphasize the importance of guest-particle size on the reduction of attraction force between metal particles, $F_{VdW,H\text{-}G}$ is calculated from Eq. (13) for a $SAC_{nom}$ of 10% for three differently sized powder fractions in Fig. 1. The Hamaker constant of the used material CoCrFeNi has been taken as that of pure iron according to the Frenkel relation ($A_{Fe} = 2.2 \cdot 10^{-19}$ J) [42,43]. The attraction force increases with increasing host-particle sizes ($D_{1,2}$), but decreases with increasing guest-particle size. The increasing spacing between host-particles, due to the presence of guest-particles, eventually runs into a minimum of the attraction force. The presence of nanoparticles prevents the contact between host-particles. However, the size of the guest-particles determines the extent of the effective adhesion reduction. The optimum guest-particle size for the minimum adhesion force is therefore also defined by the size of the host-particles [22]. From this point on, the nanoparticle coating develops its own contribution to the attraction force, guest-host interactions become pronounced. Thus, the total adhesive force increases and becomes independent of the host-particle size for these greater host-particles.

Zhu, et al. [45] describe the effect of guest-particle agglomeration on the effectiveness of adhesion reduction. The distribution of the nanoparticles is determined through the material properties and the coating procedure. The agglomeration tendency of the guest-particles leads to an increase in the effective guest-particle size and a decrease in surface area coverage. Both effects result in an increasing interparticular cohesion. The aim of the coating procedure must therefore be to deposit guest-particles as small as possible on the host surface to achieve the best possible flowability.

### 2.3. Flowability assessment

A large variety of bulk level testing methods is available for assessing the flow-improving effect of nanoparticles. In the field of AM, although there is still an ongoing discussion, about reliable analytical methods best describing the flowability of metal powders during layering macroscopically, the static and dynamic angle of repose, the latter is also known as the avalanche angle, and the bulk powder density are often used for this purpose [4]. At the microscopic scale Vallabh and Cetinkaya [46] measured the spatial adhesion distribution on a single Molybdenum microparticle via ultrasonic and surface acoustic wave based excitation techniques. Possible adhesion effects between interactions partners during AM processing were derived. Adhesion measurements of silica coated polymers with various surface coverages were performed with an atomic force microscope by Zhang, et al. [47]. They reported for an increasing nanoparticle concentration with a decreasing particle adhesion. However, in this study we used macroscopic bulk methods as they have shown to give good relative descriptions for dry-coated powders by many authors [12,16,45,48,49]. Zhou and Zhu [6] and Han, et al. [25] employed three different bulk measuring methods (avalanche angle, static angle of repose, powder rheometry) to quantify the flowability improvement of polymeric powder and glass beads with increasing nanoparticle concentration. The results showed significant differences between the static angle of repose and the higher dynamic angle of repose of 5 to 20°. However, it is stated that the measurement device should be chosen close to the powder application. It is therefore reasonable to use a measurement technique resembling the powder distribution process in an AM machine. If the flowability of metallic powders is evaluated on the basis of the dynamic angle of repose $\alpha$, recent literature is incapable of providing a limiting value $\alpha_{limit}$, below which the spreading of a powder in an LPBF machine is guaranteed. According to Carr [50], the flow behavior of powders given with the angle of repose $\alpha$ can be divided into three different classes of angles with >55° (very poor flowability), 46–55° (poor flowability) and < 45° (excellent to passable flowability).

### 2.4. Materials

#### 2.4.1. Metal powder synthesis

The host-particle material for this study ($Co_{25}Cr_{25}Fe_{25}Ni_{25}$) was melted in an alumina crucible at 1680 °C (superheating of 250 °C) and gas-atomized under Ar inert gas atmosphere. The experimental atomization set-up is further described by Schwenck, et al. [51] and Beckers,

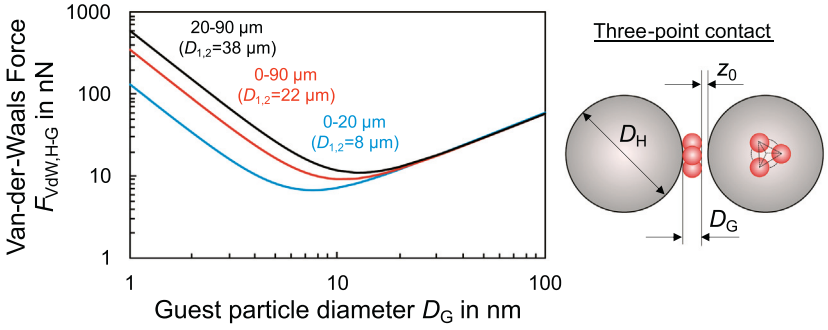


**Fig. 1.** Guest-particle ($SiO_2$) size effect on attraction force according to the three-point contact model calculated from Eq. (13) ($SAC_{nom} = 10\%$, $z_0 = 0.4 \cdot 10^{-9}$ m, $A_{SiO2} = 6.5 \cdot 10^{-19}$ J, $A_{Fe} = 2.2 \cdot 10^{-19}$ J) [43,44].

et al. [52]. Pycnometer measurements at room temperature of the fraction 0–90 μm resulted in a density of $\rho_H = 8.35 \pm 0.02$ g/cm$^3$.

### 2.5. Nanosized additive - $SiO_2$

Hydrophilic amorphous fumed silica $SiO_2$, the guest-particles in this study (Aerosil® 200) (CAS-Nr.: 772945–52-5), was purchased from Evonik Degussa GmbH. The manufacturer reports the product of flame hydrolysis of $\rho_G = 2.2$ g/cm$^3$ density to have a BET surface area $S_{BET}$ of 175–225 m$^2$/g and therefore a BET average particle size of 13.6 nm [53].

## 3. Methods

### 3.1. Powder classification

The gas atomized powder was fractionated with standard Retsch test sieves of 45, 63, 90 μm in a serial manner by separating feed amounts of 100 g (Table S1). Two fractions (0–90 μm & 0–63 μm) were air-classified under Ar inert gas atmosphere and fines <20 μm were removed. The finest size fraction 0–20 μm resulted from this separation step. These powders were named as host-particles in the following sections.

### 3.2. Particle size measurement

Particle size distribution measurements were performed with a laser diffraction instrument (Mastersizer 2000, Malvern Instruments GmbH). The powder was suspended in water at 20 °C and measured above a laser obscuration of 10%. From these measurements the host surface area $S_H$ was calculated.

### 3.3. Surface modification by dry-coating

A three-dimensional free-fall shaker mixer (Turbula T2F, WAB GmbH) was used to mix 25 g of dried (2 h at 200 °C) metal powder and nanosized $SiO_2$ in 20 ml glass containers at a rotational speed of 101 rpm. The moisture of each sample was kept as low as possible using silica gel pads. The use of a low intensity powder blender has been shown to effectively disperse nanoparticle onto host materials earlier by Zimmermann, et al. [39] and Meyer and Zimmermann [54] and more recently by Sunkara and Capece [20].

The effect of additional nanoparticles on the metal powder flow behavior was investigated for various nanoparticle concentrations. The powders were mixed for 20 min with increasing nanoparticle concentration (Table S2). The flowability was also studied for increasing mixing times ($t_{mix} = 2$; 6; 20; 60; 180; 360; 1440 min) at a constant $SAC_{nom}$ of 128 ± 5% ($w_{SiO2/(0–90μm)} = 0.067 \pm 0.001$ wt.-% / $w_{SiO2/(20–90μm)} = 0.043 \pm 0.001$ wt.-%) for two different powders (0–90 μm / 20–90 μm) (Table S3). In this case the Sauter mean diameter of the 0–90 μm fraction was $D_{1,2} = 25$ μm.

### 3.4. Morphology and surface characterization with SEM and AFM

Scanning electron microscopy (SEM) images were acquired with a ZEISS-SUPRA40 equipped with Inlense and secondary electron (SE) detectors. For the qualitative observation an accelerating voltage of 2 kV (Inlense) & 7 kV (SE) and a working distance of 2.9 mm (Inlense) & 7.1 mm (SE) were employed.

Surface topography scans (4 × 4 μm) of 15–20 μm sized single particles of fraction 0–90 μm were performed in air with atomic force microscopy (AFM) (Nanowizard 3, JPK) in tapping mode at room temperature. Silicon probes of type TESPV-2 (320 kHz, 42 N/m) were used for AFM imaging. The tapping frequency was set to 300.841 kHz with a phase shift of −167° and a drive amplitude of 0.04 V. Subsequent to the scanning of the sample, the curvature of the spherical particle could be eliminated by means of 2nd degree polynomial background removal using the free-access software Gwyddion. Single representative height profiles were extracted.

### 3.5. Flowability characterization

The dynamic flow test was performed with a self-designed device consisting of a CCD-camera (26 frames per second), a motorized powder drum and a light source, which were placed on an optical bench. The powder drum with a diameter of 31 mm and length of 25 mm was filled with 25 g powder mass. The dynamic angle of repose $\alpha$ was determined with recording the avalanching powder and calculating the average angle of the upper powder skin towards the lowest avalanche point and the intersecting horizontal plane at a rotation speed of 5 rpm. When the powder showed an average angle larger than 55°, manual measurements of at least 10 avalanches were performed. The bulk powder densities $\rho_B$ were measured with pouring the metal powders into a 10 ml flask and manually reading the pile surface top.

## 4. Results and discussion

### 4.1. Size and morphology of raw uncoated powders (host-particle)

The PSDs of all powders are shown in Fig. 2 according to their cumulative powder volume $Q_3$ of each particle class and characteristic values are summarized in Table S1. To describe a PSD different characteristic values are available. Often in LPBF related publications local values of the volume-based distribution are used, such as the mass median particle size $D_{50,3}$, or similarly $D_{10,3}$ and $D_{90,3}$. These values refer to the particle size at which a certain percentage of a distribution is smaller than a specific size, however, distribution width and shape are not taken into account by these characteristics. To ensure comparability between the fractions the Sauter diameter $D_{1,2}$ is used. This work investigates the effect of dry-coating on the dynamic angle of repose and the bulk powder density of powders containing different amounts of fine particles <20 μm. One set of powders $D_{1,2} = 33$ μm (20–63 μm) and $D_{1,2} = 38$ μm (20–90 μm) contained low amounts of fines <20 μm of 8 vol.-%. The other set $D_{1,2} = 22$ μm (0–90 μm), $D_{1,2} = 19$ μm (0–63 μm), $D_{1,2} = 16$ μm (0–45 μm) and $D_{1,2} = 8$ μm (0–20 μm) showed steadily increasing amounts of fines <20 μm from 23 to 95 vol.-% and decreasing upper particle sizes, respectively.

SEM images confirm predominantly spherical shape with only very few satellite structures present (Fig. 3). The surface of all powders appears free of pores and relativity smooth. In summary, powders with varying average particle size and quantity of fine particles <20 μm with spherical shape were produced.

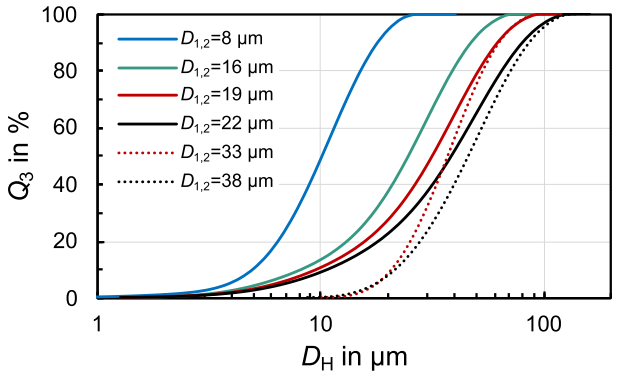


**Fig. 2.** Volume $Q_3$ based cumulative particle size distribution of CoCrFeNi powders.

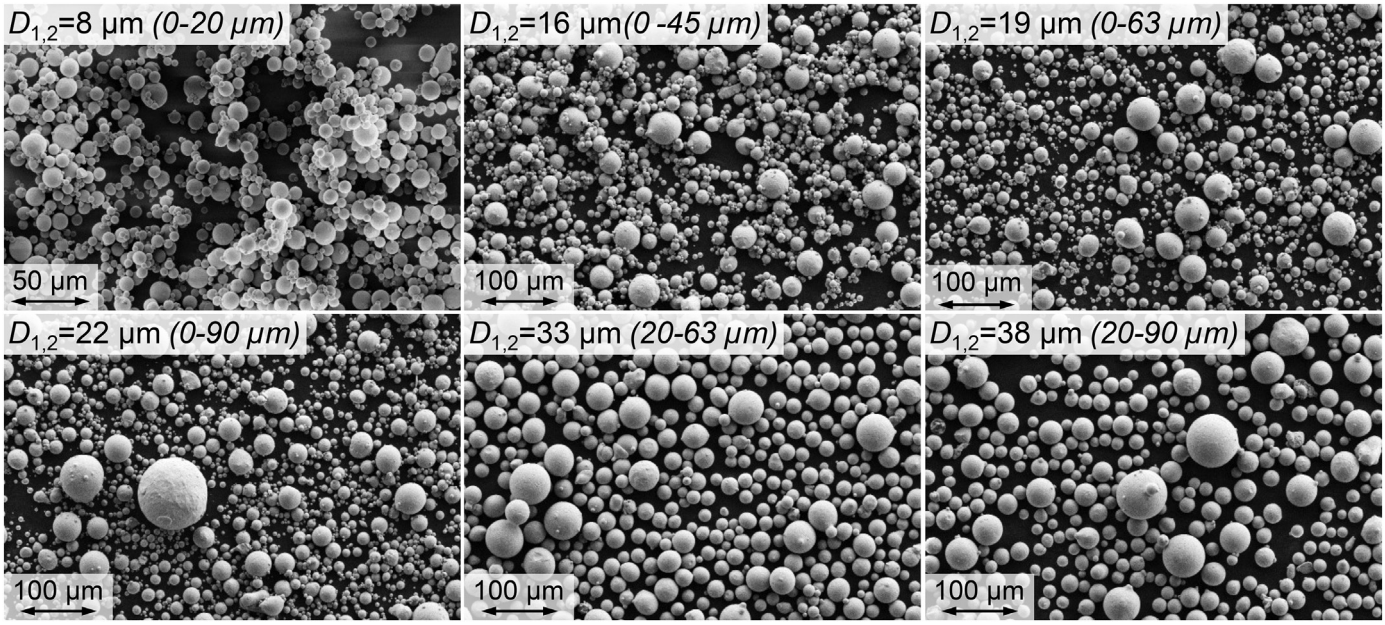


**Fig. 3.** SEM images of uncoated CoCrFeNi powders of different size distributions. The scaling of the finest powder $D_{1,2} = 8$ µm is 50 µm in comparison to 100 µm of all other fractions.

*4.2. Nanoparticle concentration effect on flowability*

The effect of the nanoparticle concentration and its contribution to the flow behavior of the CoCrFeNi powder was studied with a nominal $SAC_{nom}$ between 4 and 300% at a constant mixing time of 20 min. The dynamic angle of repose and the bulk powder density were measured. Since nanoparticle agglomeration is often observed in dry-coating [55,56], $SAC_{nom}$ was raised well above 100%. Increasing the nanoparticle $SAC$ of all powders led to a decreasing dynamic angle of repose $\alpha$ (Fig. 4). Each data point in the diagram represents one mixing experiment. Uncoated fractions containing fines <20 µm ($D_{1,2} < 23$ µm) show a high dynamic angle of repose of 63–78°. According to Carr [50] such a flowability can be ranked as 'very poor'. If the fine fraction is removed, the angle $\alpha$ reduces to 55° and 45° for LPBF fractions $D_{1,2} = 33$ µm (20–63 µm) and $D_{1,2} = 38$ µm (20–90 µm). Both powders were spread horizontally with a brush like feeder in a LPBF machine (Aconity Mini, Aconity GmbH). The finer powder $D_{1,2} = 33$ µm (20–63 µm) qualitatively showed a tendency to inhomogeneous powder layering as powder lumps and cm-sized uncovered areas in the powder layer were visible from spreading a 50 µm layer. In comparison, the powder $D_{1,2} = 38$ µm (20–90 µm) was well spreadable without any layer imperfections. Therefore, the arithmetic mean of the dynamic angle of repose between both powders is considered the limiting value $\alpha_{Limit} = 50°$ and is assigned for the minimum necessary dynamic angle of repose for LPBF applications. This is in good agreement with the flowability categorization according to Carr [50], who differentiates between 'poor' and 'very poor' flowability for critical static angles of repose above and below 55°, respectively. Once coated, the dynamic angle of repose of all powders declines below $\alpha_{Limit}$ with increasing nanoparticle concentration. In a first region of lower nominal nanoparticle $SAC_{nom}$, relatively large changes of the dynamic angle of repose until approximately 20–25% $SAC_{nom}$ were observed for powders containing fines <20 µm. Fractions without fines were less significantly altered with the addition of nanoparticles as their initial uncoated flow behavior is already considered 'better flowing'. In a second region, moderate changes were detected, indicating a maximum flowability enhancement with increasing surface coverage of nanoparticles. The error bars originate from the measurement of the dynamic angle of repose of at least 10 avalanches. The variations of the dynamic angle of repose within each mixing experiment generally decreases with increasing flowability.

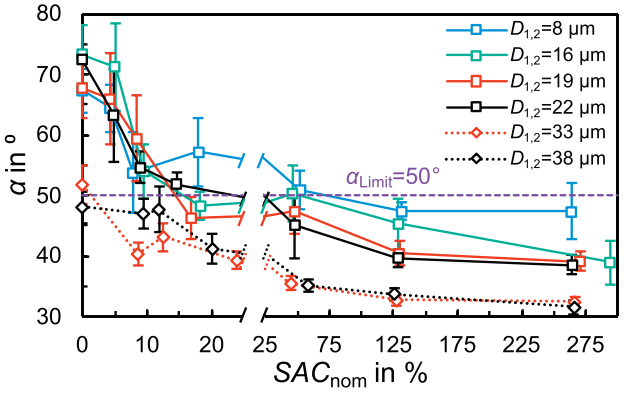


**Fig. 4.** Dynamic angle of repose $\alpha$ of CoCrFeNi coated with $SiO_2$ at 20 min mixing time with two differently scaled $SAC_{nom}$ regions from 0 to 25% and 25 to 300%.

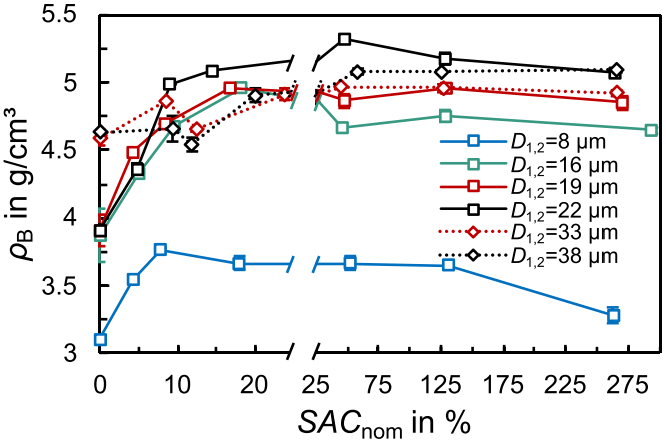


**Fig. 5.** Bulk powder density $\rho_B$ of uncoated and coated CoCrFeNi for a 20 min mixing time with two differently scaled $SAC_{nom}$ regions from 0 to 25% and 25 to 300%.

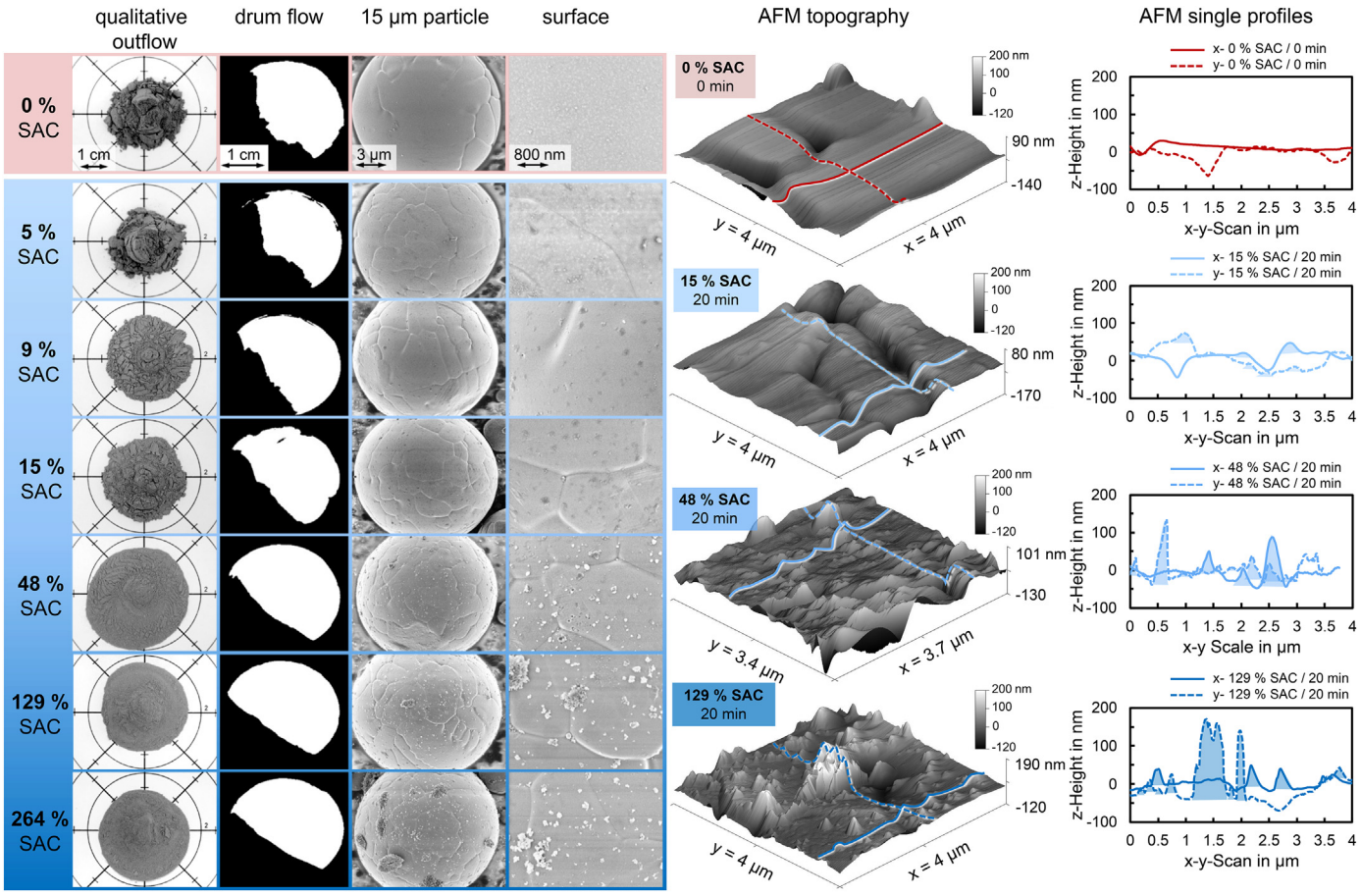


**Fig. 6.** $SAC_{nom}$ dependent flowability images, surface morphology and AFM surface topographies of single particles of fraction 0–90 µm ($D_{1,2} = 22$ µm) at 20 min mixing time. The shaded areas in the AFM single profiles are assigned to the nanoparticle coverage.

In order to determine the coating effect on the powder bed, the bulk powder densities were measured (Fig. 5). Without dry-coating, the fraction $D_{1,2} = 8$ µm showed the lowest bulk powder density $\rho_B$ of 3.1 g/cm$^3$. Increasing the Sauter diameter led to denser powder packing and higher bulk powder densities for the uncoated fractions $D_{1,2} = 8$ µm, $D_{1,2} = 16$ µm, $D_{1,2} = 19$ µm and $D_{1,2} = 22$ µm. Removing the fine powder <20 µm further increased the powder packing for conventional LPBF fractions as high as 4.6 g/cm$^3$. The data showed only slight deviations within each mixing experiment resulting in small error bars. For all powders, there was already a detectable increase in bulk powder density $\rho_B$ at low concentrations of nanoparticles up to 10% *SAC*. Further increasing the $SAC_{nom}$ resulted only in minor changes and solely for the smallest powder the decrease was relevant.

With close examination of the host surface (SEM and AFM) and the resulting flow behavior (images of qualitative funnel outflow and dynamic angle of repose) of fraction $D_{1,2} = 22$ µm (0–90 µm) a clear shift in guest-particle arrangement from patch-like to loosely adhering aggregates was observed (Fig. 6). The uncoated surface was smooth and AFM topography scans showed microscopic depressions in the range of 80 nm. From this smooth and even surface strong interparticle forces result in low flowability. At low $SAC_{nom}$ (<15%), an increasing concentration of darker patch-like nanoparticle aggregates is seen from SEM micrographs and additional roughness in the tens of nanometer was detected in AFM topographies. With further increasing nanoparticle concentration (>48% *SAC*) more loosely bonded nanoparticle aggregates of varying size, between 10 and 100 nm, were dispersed on the host surface. At high $SAC_{nom}$ (>128%) aggregates and micrometer sized agglomerates are found on the host surfaces as a result of insufficient deagglomeration. The nanoparticles can adhere to the host-particles as well as to each other because of various interaction forces. Since the nanoparticles were processed under ambient conditions and a relative humidity greater than zero, water vapor condensation on the nanoparticle surface is expected. This causes the formation

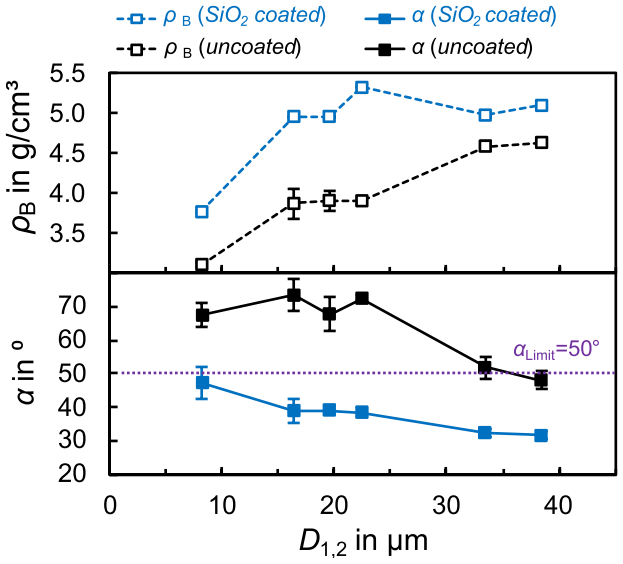


**Fig. 7.** Bulk powder density $\rho_B$ (top) and dynamic angle of repose $\alpha$ (bottom) of each powder upon 129 ± 5% $SAC_{nom}$ $SiO_2$ coating for 20 min.

of a structured water molecular layer on the nanoparticle surface [57]. The resulting solvation and capillary forces dominate the overall adhesion characteristics of the interaction forces [58].

Meyer and Zimmermann [54] predicted the maximum reduction of Van-der-Waals force once the transition from guest-host to guest-guest contacts occurs at a $SAC_{nom}$ of 45.3%. At this concentration, the nanoparticles should arrange themselves uniformly in a hexagonal pattern in a monolayer. However, our surface analyses revealed a formation of differently structured aggregates, resulting in drastically lower real $SAC_{real}$. Still, the flowability was significantly affected, such that after a $SAC_{nom}$ of 129% only slight reductions of the dynamic angle of repose were observed. It is therefore reasonable to assume, that the attraction force has been minimized through the additional roughness of the nanoparticle coating and inertial forces have a more pronounced effect on the flowability. In Fig. 7 uncoated and coated (129% $SAC_{nom}$) powders are compared. The weight force scales with the host-particle size resulting in denser powder packing and improved flowability with increasing particle size. In cases where guest-particle coatings were applied, powder densities and the dynamic angle of repose continued to this trend.

Following the concept of calculating the acting force ratio on uncoated and coated metal particles from Eq. (5) and Eq. (13), the granular Bond number $Bo_{Granu}$ is correlated with the powder flow performance in Fig. 8. The surface analyses showed strong deviations between the nominal $SAC_{nom}$ and a real coverage $SAC_{real}$ distributed on the metal particle surface. From image analyses of single SEM micrographs an average real $SAC_{real}$ of 5% and the agglomerated guest-particle size $D_{G,aggl}$ of 100 nm were deduced (Table S4).

Similar to Capece, et al. [18], we used an empirical power law expression to correlate the dynamic angle of repose and the computed $Bo_{Granu}$ according to the Sauter diameter of the powder. The best fit was found for the fitting parameters a = 21.40 and b = 0.13 with $R^2$ = 0.84 based on the calculation of smooth, uncoated host-particles and the three-point contact model when coated.

$$\alpha = a(Bo_{Granu})^b \tag{16}$$

Discrepancies from the fit were observed for the dynamic angle of repose greater than or equal $\alpha_{Limit}$. As dry-coating also showed a strong

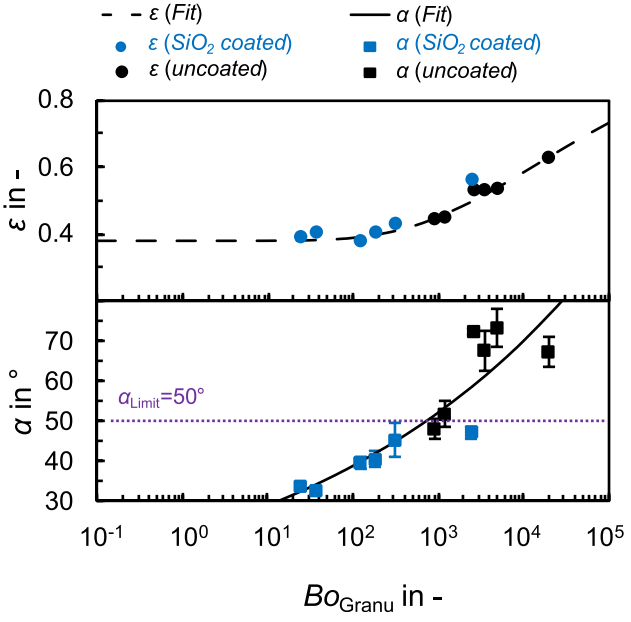


**Fig. 8.** Powder porosity $\varepsilon$ (top) and dynamic angle of repose $\alpha$ (bottom) as a function of the granular Bond-number $Bo_{Granu}$ calculated from Eqs. (1) and (13) for $SAC_{real} = 5\% < SAC_{G\text{-}G}$ and $D_{G,aggl}$ = 100 nm approximated from SEM image analysis.

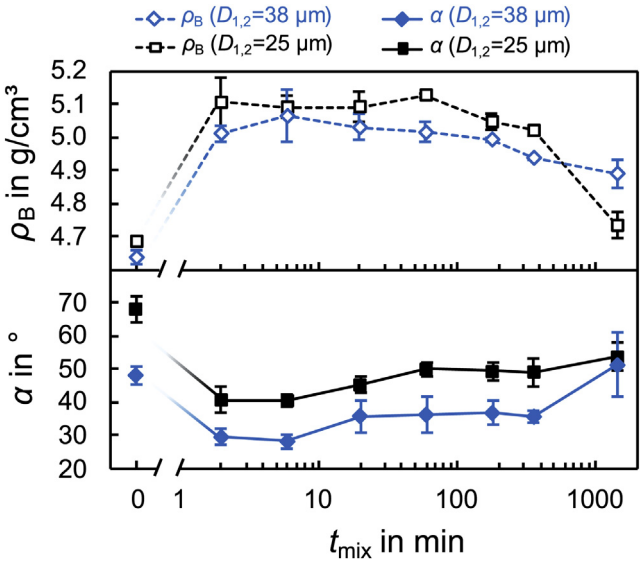


**Fig. 9.** Bulk powder density $\rho_B$ (top) and dynamic angle of repose $\alpha$ (bottom) of fraction 0–90 µm ($D_{1,2}$ = 25 µm) and 20–90 µm ($D_{1,2}$ = 38 µm) at ~128 ± 5% $SAC_{nom}$ for different mixing times.

altering effect on the bulk powder density, we compared the powder bed porosity $\varepsilon$ of Eq. (4) proposed by Yu, et al. [29] with computations of $Bo_{Granu}$. This relation proved particularly useful for correlating our results for metal powders with the governing forces of dry-coated particles. We found the best fit for $n$ = 0.27 and m = 13.06. The $\varepsilon_0$ was set to 0.38. With the assumptions made from Capece, et al. [9], the best fit of Eq. (4) with our data set was obtained with $n$ = 0.20 and m = 3.84, which is in good agreement with the original literature.

### 4.3. Mixing time dependency of coated powders

Variations of the nanoparticle concentration resulted in different sizes and arrangements of the guest-particles on the host surfaces. The process kinetics of dry-coating an assembly of guest-particle aggregates can be separated into two regimes according to Blümel [56]: (i) coating (increasing aggregate concentration) and (ii) decoating (decreasing aggregate concentration). To account for the effect of mixing time, the powder flowability and bulk powder density were investigated for mixing times varying from 2 to 1440 min (24 h) (Fig. 9). These experiments were performed using two powder fractions with low (20–90 µm, $D_{1,2}$ = 38 µm) and high amount of fines <20 µm (0–90 µm, $D_{1,2}$ = 25 µm), respectively, while maintaining a constant nanoparticle load ($SAC_{nom}$ = 128 ± 5%). The surface loading was chosen to ensure that sufficient guest-particles were available for a maximum force reduction. A maximum reduction of the dynamic angle of repose occurred from 65 to 40° for the fine $D_{1,2}$ = 25 µm and 48 to 28° for the coarser fraction $D_{1,2}$ = 38 µm after 6 min of mixing. Similarly, the bulk powder densities increased from 4.68 to 5.10 g/cm³ (fine) and 4.63 to 5.03 g/cm³ (coarse), respectively. Longer mixing times of up to 360 min caused a significant increase of the dynamic angle of repose and a slightly decreasing powder bulk density of $D_{1,2}$ = 38 µm. However, the powder packing of $D_{1,2}$ = 25 µm remained unaffected. Excessive mixing until 1440 min yielded a dynamic angle of repose of 51° exceeding the value of the uncoated powder of the fraction $D_{1,2}$ = 38 µm. Reduced bulk powder densities were found for both fractions, although more pronounced for the fraction with fines $D_{1,2}$ = 25 µm. At long mixing times the dry-coated powders surpassed $\alpha_{Limit}$ again and their flowability was too low for LPBF processing.

The surface analyses of fraction $D_{1,2}$ = 25 µm showed changing guest-particle arrangements as result of increasing mixing time

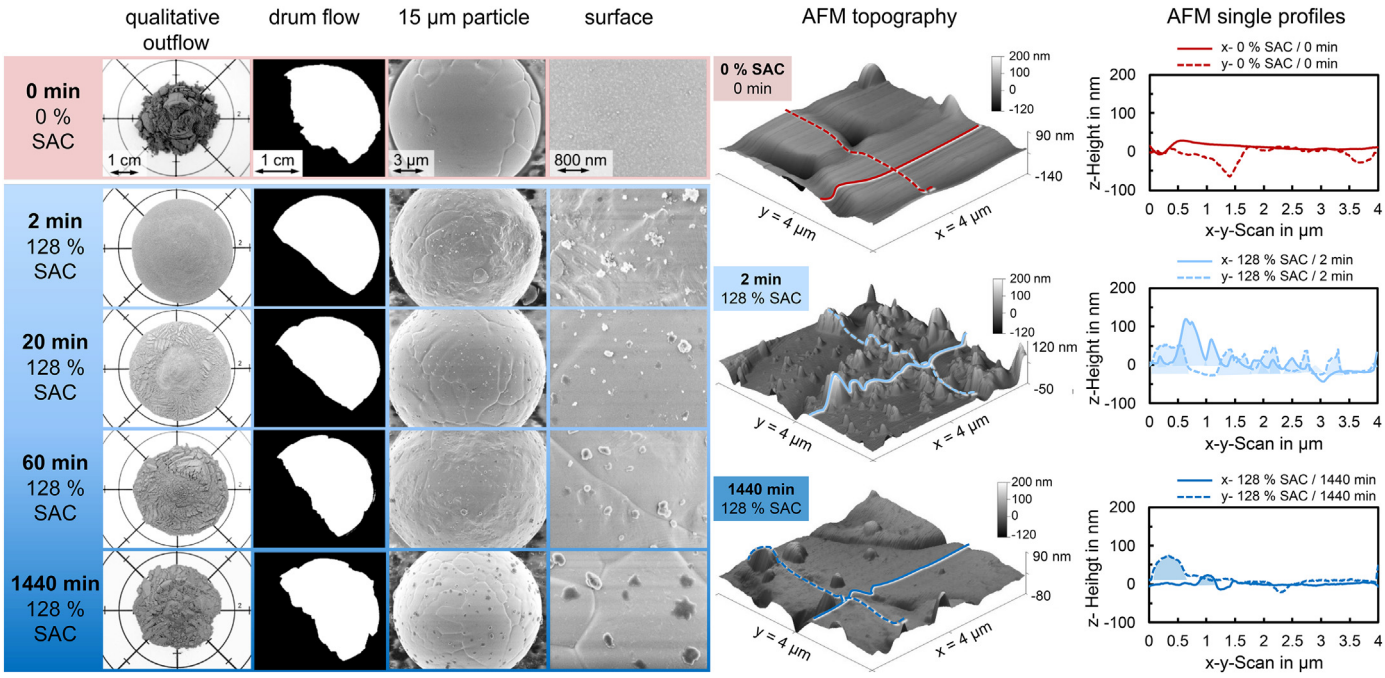


**Fig. 10.** Mixing time dependent flowability images, surface morphology and AFM surface topographies of single particles of fraction 0–90 µm ($D_{1,2} = 25$ µm) at ~128 ± 5% $SAC_{nom}$. The shaded areas in the AFM single profiles are assigned to the nanoparticle coverage.

(Fig. 10). At a short mixing time of 2 min, micrometer-sized $SiO_2$ agglomerates are broken up between colliding metal particles [19,59]. The shearing fragments from the collisions loosely adhere to the surface of the host-particles as aggregates of 20 to 110 nm size (AFM height) with relatively small distances to each other (see AFM profile for 2 min mixing time). The homogeneously distributed guest-particle aggregates prevent further host-contacts and moreover increase the contact distance. Consequently, the attraction forces are reduced, resulting in a strong decrease of the dynamic angle of repose and increase of the bulk powder density [15,54]. The number of collisions between metal particles and adhering guest-particle structures increases for longer mixing times. Reagglomeration or decoating was seen at 20 and 60 min evident from the larger aggregate size (≈ 150 nm, estimated from SEM micrographs) and lower aggregate concentration on the host surface. When the size of the guest-particle aggregates increases, the Van-der-Waals force determining host-guest interaction simultaneously increases (see Fig. 1). Therefore, the powder flowability decreases. Exceptionally long mixing times increased the effect of reagglomeration, further decreased the number of guest-particle aggregates and caused the compaction of agglomerates into patch-like structures of narrow height (30 to 80 nm) and hundreds of nanometers lateral expansion. As a result, the distances between $SiO_2$ guest-particles has increased and host-particle contacts are less effectively prevented. An increasing cohesiveness of the metal powders was observed [45].

Unlike often reported in literature [21,22,39,48,49,54,60] an inhomogeneous discrete coating rather than a continuous coating or even film of nanoparticles was observed with different experimental techniques in this study. The metal powder used in this work had a density of about 8.35 g/cm$^3$, which is approximately four times higher compared to host powders used in the pharmaceutical industry, from which most of the literature originates. In a free-fall shaker mixer metal particles of high kinetic energy during the fall will more effectively disintegrate initial nanoparticle agglomerates into aggregates adhering on the host surface during mixing. Meyer and Zimmermann [54] show for a similar mixing process and nanoparticles but less dense host-particles (cornstarch with a density of 0.5–1.5 g/cm$^3$) a much slower kinetic of the improvement of powder flowability. This leads to our assumption, that in a free-fall situation the deagglomeration of nanoparticles is driven from the density and therefore kinetic energy of the host-particles. Since high surface concentrations of guest-particle aggregates are favorable for the reduction of Van-der-Waals force [56], shorter mixing times are preferable for metal powders, due to the inherent mixing energy of the metal powders. Therefore, dry-coated metal powders with low $SAC_{nom}$ (< 20%) showed a less pronounced flow improvement, when extensively mixed. Reduced mixing times will increase their effectiveness on the reduction of powder cohesion.

## 5. Conclusions

The capabilities of conditioning AM powders with dry-coating of nanoparticles was demonstrated for different powder fractions <90 µm of an equimolar alloy metal powder (CoCrFeNi). Dry-coating with ~13 nm sized $SiO_2$ nanoparticles led to a substantial improvement of flowability and bulk powder density. The functionalization of all studied fractions decreased the dynamic angle of repose below 50° and an overall reduction of nearly 30 to 50% was achieved. The bulk powder densities of fractions containing high amounts of fines <20 µm between 23 and 95 vol.-% were increased by 20–30%. The preserved fine fraction clearly demonstrates the potential of nanoparticle dry-coating for AM technologies. Coarser fractions that are more common in LPBF (20–63 µm and 20–90 µm) were densified by 10%. Low amounts (0.03 to 0.2 wt.-%) of nanoscale $SiO_2$ resulted in a reduction of the distance-controlled Van-der-Waals force and enhanced powder flowability and packing. The flow performance und powder bed porosity of uncoated and coated powders was successfully described with the granular Bond number $Bo_{Granu}$ for metallic powders. The obtained correlations were in good agreement with respect to literature findings for non-metallic materials. SEM and AFM analyses of metal powder surfaces revealed that the effectiveness of the coating is determined by agglomeration of the nanoscale additives. Both the nanoparticle concentration and the mixing time are critical process-determining factors. Best coating results were achieved for short mixing times up to 6

min. Intensive mixing over a longer period (1 to 24 h) caused reagglomeration of the nanoparticles. The cohesion-reducing effect of the artificial roughness diminished and the powder performance was reduced.

Supplementary data to this article can be found online at https://doi.org/10.1016/j.powtec.2020.10.065.

## Declaration of Competing Interest

The authors declare that they have no known competing financial interests or personal relationships that could have appeared to influence the work reported in this paper.

The authors declare the following financial interests/personal relationships which may be considered as potential competing interests:

## Acknowledgment

We would like to thank the German research foundation for the financial support and members of the SPP 2006 (funding number UH 77/11-1, DE 796/13-1, JA 2482/3-1). The authors thank Nils Ellendt for scientific discussions and Coucong Gong for the support with AFM topography measurements.

## References

[1] P.K. Gokuldoss, S. Kolla, J. Eckert, Additive manufacturing processes: selective laser melting, Electron beam melting and binder jetting-selection guidelines, Materials (Basel) 10 (2017) 672.
[2] D. Gu, W. Meiners, K. Wissenbach, R. Poprawe, Laser additive manufacturing of metallic components: materials, processes and mechanisms, Int. Mater. Rev. 57 (2012) 133–164.
[3] D. Herzog, V. Seyda, E. Wycisk, C. Emmelmann, Additive manufacturing of metals, Acta Mater. 117 (2016) 371–392.
[4] S. Vock, B. Klöden, A. Kirchner, T. Weißgärber, B. Kieback, Powders for powder bed fusion: a review, Prog. Add. Manufact. 4 (2019) 383–397.
[5] D. Geldart, Types of gas fluidization, Powder Technol. 7 (1973) 285–292.
[6] Y. Zhou, J. Zhu, Group C+ particles: enhanced flow and fluidization of fine powders with nano-modulation, Chem. Eng. Sci. 207 (2019) 653–662.
[7] L.I. Escano, N.D. Parab, L. Xiong, Q. Guo, C. Zhao, K. Fezzaa, W. Everhart, T. Sun, L. Chen, Revealing particle-scale powder spreading dynamics in powder-bed-based additive manufacturing process by high-speed x-ray imaging, Sci. Rep. 8 (2018) 15079.
[8] B. Ma, Q. Jiang, J. Huang, X. Wang, J. Leng, Effect of different silica particles on flowability of gypsum powder for 3D powder printing, Constr. Build. Mater. 217 (2019) 394–402.
[9] M. Capece, Z. Huang, D. To, M. Aloia, C. Muchira, R.N. Davé, A.B. Yu, Prediction of porosity from particle scale interactions: surface modification of fine cohesive powders, Powder Technol. 254 (2014) 103–113.
[10] D.J. McClements, H. Xiao, Is nano safe in foods? Establishing the factors impacting the gastrointestinal fate and toxicity of organic and inorganic food-grade nanoparticles, Sci. Food 1 (2017) 6.
[11] K. Siliveru, C.G. Jange, J.W. Kwek, R.P.K. Ambrose, Granular bond number model to predict the flow of fine flour powders using particle properties, J. Food Eng. 208 (2017) 11–18.
[12] Q. Li, V. Rudolph, B. Weigl, A. Earl, Interparticle van der Waals force in powder flowability and compactibility, Int. J. Pharm. 280 (2004) 77–93.
[13] D. Schulze, Pulver und Schüttgüter: Fließeigenschaften und Handhabung, 3., erg. Aufl. Springer Vieweg, Berlin, 2014.
[14] R. Sharma, G. Setia, Mechanical dry particle coating on cohesive pharmaceutical powders for improving flowability - a review, Powder Technol. 356 (2019) 458–479.
[15] A. Castellanos, The relationship between attractive interparticle forces and bulk behaviour in dry and uncharged fine powders, Adv. Phys. 54 (2005) 263–376.
[16] M.C.H. Karg, A. Munk, B. Ahuja, M.V. Backer, J.P. Schmitt, C. Stengel, S.V. Kuryntsev, M. Schmidt, Expanding particle size distribution and morphology of aluminium-silicon powders for laser beam melting by dry coating with silica nanoparticles, J. Mater. Process. Technol. 264 (2019) 155–171.
[17] R. Streubel, M.B. Wilms, C. Doñate-Buendía, A. Weisheit, S. Barcikowski, J.H. Schleifenbaum, B. Gökce, Depositing laser-generated nanoparticles on powders for additive manufacturing of oxide dispersed strengthened alloy parts via laser metal deposition, Japanese J. Appl. Phys. 57 (2018) 040310-040311–040310-040310.
[18] M. Capece, R. Ho, J. Strong, P. Gao, Prediction of powder flow performance using a multi-component granular bond number, Powder Technol. 286 (2015) 561–571.
[19] W. Kaialy, On the effects of blending, physicochemical properties, and their interactions on the performance of carrier-based dry powders for inhalation — a review, Adv. Coll. Interfac 235 (2016) 70–89.
[20] D. Sunkara, M. Capece, Influence of material properties on the effectiveness of glidants used to improve the flowability of cohesive pharmaceutical powders, AAPS PharmSciTech 19 (2018) 1920–1930.
[21] Z. Huang, J.V. Scicolone, L. Gurumuthy, R.N. Davé, Flow and bulk density enhancements of pharmaceutical powders using a conical screen mill: a continuous dry coating device, Chem. Eng. Sci. 125 (2015) 209–224.
[22] J. Yang, A. Sliva, A. Banerjee, R.N. Dave, R. Pfeffer, Dry particle coating for improving the flowability of cohesive powders, Powder Technol. 158 (2005) 21–33.
[23] Q. Huang, H. Zhang, J. Zhu, Flow properties of fine powders in powder coating, Particuology 8 (2010) 19–27.
[24] C.C. Xu, H. Zhang, J. Zhu, Improving flowability of cohesive particles by partial coating on the surfaces, Can. J. Chem. Eng. 87 (2009) 403–414.
[25] M. Han, Y. Zhou, J. Zhu, Improvement on flowability and fluidization of group C particles after nanoparticle modification, Powder Technol. 365 (2020) 208–214.
[26] Y. Chen, L. Jallo, M.A.S. Quintanilla, R. Dave, Characterization of particle and bulk level cohesion reduction of surface modified fine aluminum powders, Colloids Surf. A Physicochem. Eng. Asp. 361 (2010) 66–80.
[27] L.J. Jallo, Y. Chen, J. Bowen, F. Etzler, R. Dave, Prediction of inter-particle adhesion force from surface energy and surface roughness, J. Adhes. Sci. Technol. 25 (2011) 367–384.
[28] M. Capece, K.R. Silva, D. Sunkara, J. Strong, P. Gao, On the relationship of inter-particle cohesiveness and bulk powder behavior: Flowability of pharmaceutical powders, Int. J. Pharm. 511 (2016) 178–189.
[29] A.B. Yu, C.L. Feng, R.P. Zou, R.Y. Yang, On the relationship between porosity and interparticle forces, Powder Technol. 130 (2003) 70–76.
[30] C. Blümel, M. Sachs, T. Laumer, B. Winzer, J. Schmidt, M. Schmidt, W. Peukert, K.E. Wirth, Increasing flowability and bulk density of PE-HD powders by a dry particle coating process and impact on LBM processes, Rapid Prototyp. J. 21 (2015) 697–704.
[31] W. Peng, G. Wang, M.F.X. Gigliotti Jr., P. Singh, E.P. Office, Method for treating powder and powder treated thereby, 2016.
[32] M. Melnichuk, D.J. Cuscueta, N. Silin, Effect of glidants on LaNi5 powder flowability, Int. J. Hydrog. Energy 43 (2018) 6219–6228.
[33] M.C.H. Karg, M. Rasch, K. Schmidt, S.A.E. Spitzer, T.F. Karsten, D. Schlaug, C.-R. Biaciu, A.I. Gorunov, M. Schmidt, et al., Nanomaterials (Basel, Switzerland) 8 (2018) 862.
[34] S. Kleinschmidt, J. Tomas, Verbesserung der Fließfähigkeit feiner kohäsiver Pulver durch nanoskalige Fließhilfsmittel, Chemie Ingenieur Technik 81 (2009) 717–733.
[35] H. Rumpf, Grundlagen und methoden des granulierens, Chemie Ingenieur Technik 30 (1958) 144–158.
[36] Y. Chen, J. Yang, R.N. Dave, R. Pfeffer, Fluidization of coated group C powders, AIChE J. 54 (2008) 104–121.
[37] H. Rumpf, Die wissenschaft des agglomerierens, Chemie Ingenieur Technik 46 (1974) 1–11.
[38] E.R. Beach, G.W. Tormoen, J. Drelich, R. Han, Pull-off force measurements between rough surfaces by atomic force microscopy, J. Colloid Interface Sci. 247 (2002) 84–99.
[39] I. Zimmermann, M. Eber, K. Meyer, Nanomaterials as flow regulators in dry powders, Zeitschrift für Physikalische, Chemie (2004) 51.
[40] K. Meyer, Nanomaterialien als Fließregulierungsmittel, Universität Würzburg, Fakultät für Chemie und Pharmazie, Fakultät für Chemie und Pharmazie/Institut für Pharmazie und Lebensmittelchemie, 2003.
[41] Y. Chen, M.A.S. Quintanilla, J. Yang, J.M. Valverde, R.N. Dave, Pull-off force of coated fine powders under small consolidation, Phys. Rev. E 79 (2009) 041305-041301–041305-041314.
[42] J.N. Israelachvili, Intermolecular and Surface Forces, 3rd ed. Academic Press, Burlington, MA, 2011.
[43] F.M. Fowkes, Attractive forces at interfaces, Ind. Eng. Chem. 56 (1964) 40–52.
[44] L. Bergström, Hamaker constants of inorganic materials, Adv. Coll. Interfac 70 (1997) 125–169.
[45] X. Zhu, Q. Zhang, C. Huang, Y. Wang, C. Yang, F. Wei, Validation of surface coating with nanoparticles to improve the flowability of fine cohesive powders, Particuology 30 (2017) 53–61.
[46] C.K.P. Vallabh, C. Cetinkaya, Single particle adhesion variability in additive manufacturing powders, J. Adhes. (2019) 1–19.
[47] H. Zhang, W. Ding, C. Cetinkaya, Effects of nanoparticle coverage on the adhesion properties of emulsion aggregation toner particles, J. Imag. Sci. Technol. 54 (2010) 20501-20501–20501-20507.
[48] F. Fulchini, U. Zafar, C. Hare, M. Ghadiri, H. Tantawy, H. Ahmadian, M. Poletto, Relationship between surface area coverage of flow-aids and flowability of cohesive particles, Powder Technol. 322 (2017) 417–427.
[49] L.J. Jallo, C. Ghoroi, L. Gurumurthy, U. Patel, R.N. Dave, Improvement of flow and bulk density of pharmaceutical powders using surface modification, Int. J. Pharm. 423 (2012) 213–225.
[50] R.L. Carr, Evaluating flow properties of solids, Chem. Eng. 72 (1965) 163–168.
[51] D. Schwenck, N. Ellendt, J. Fischer-Bühner, P. Hofmann, V. Uhlenwinkel, A novel convergent–divergent annular nozzle design for close-coupled atomisation, Powder Metall. 60 (2017) 198–207.
[52] D. Beckers, N. Ellendt, U. Fritsching, V. Uhlenwinkel, Impact of process flow conditions on particle morphology in metal powder production via gas atomization, Adv. Powder Technol. 31 (2020) 300–311.
[53] E.D. GmbH, Aerosil - Fumed Silica - Technical Overview, 2019.
[54] K. Meyer, I. Zimmermann, Effect of glidants in binary powder mixtures, Powder Technol. 139 (2004) 40–54.
[55] X. Deng, R.N. Davé, Adhesion and friction of dry-coated nano-rough particles, Powder Technol. 314 (2017) 20–27.

[56] C. Blümel, Charakterisierung der Trockenen Beschichtung zur Herstellung von maßgeschneiderten Kompositpartikeln, Friedrich-Alexander-Universität Erlangen Nürnberg, 2015.
[57] J. Laube, S. Salameh, M. Kappl, L. Mädler, L. Colombi Ciacchi, Contact forces between TiO2 nanoparticles governed by an interplay of adsorbed water layers and roughness, Langmuir 31 (2015) 11288–11295.
[58] V. Baric, J. Laube, S. Salameh, L. Colombi Ciacchi, L. Mädler, A contact model for the discrete element simulations of aggregated nanoparticle films, in: S. Antonyuk (Ed.), Particles in Contact: Micro Mechanics, Springer International Publishing, Cham, Micro Process Dynamics and Particle Collective 2019, pp. 339–358.
[59] M.R. Tamadondar, L. de Martín, K. Thalberg, I.N. Björn, A. Rasmuson, The influence of particle interfacial energies and mixing energy on the mixture quality of the dry-coating process, Powder Technol. 338 (2018) 313–324.
[60] V. Karde, S. Panda, C. Ghoroi, Surface modification to improve powder bulk behavior under humid conditions, Powder Technol. 278 (2015) 181–188.